

Third-order nonlinear wavelength conversion in chalcogenide glass waveguides towards mid-infrared photonics

Fengbo Han(韩锋博), Jiaxin Gu(顾佳新), Lu Huang(黄璐), Hang Wang(王航), Yali Huang(黄雅莉), Xuecheng Zhou(周学成), Shaoliang Yu(虞绍良), Zhengqian Luo(罗正钱), Zhipeng Dong(董志鹏), and Qingyang Du(杜清扬)
Citation: Chin. Phys. B, 2024, 33 (**10**): 104207. DOI: 10.1088/1674-1056/ad6557
Journal homepage: http://cpb.iphy.ac.cn; http://iopscience.iop.org/cpb

What follows is a list of articles you may be interested in

Generation of mid-infrared supercontinuum by designing circular photonic crystal fiber

Ying Huang(黄颖), Hua Yang(杨华), and Yucheng Mao(毛雨澄)
Chin. Phys. B, 2022, 31 (**5**): 054211. DOI: 10.1088/1674-1056/ac272c

Ultrabroadband mid-infrared emission from Cr^{2+}:ZnSe-doped chalcogenide glasses prepared via hot uniaxial pressing and melt-quenching

Ke-Lun Xia(夏克伦), Guang Jia(贾光), Hao-Tian Gan(甘浩天), Yi-Ming Gui(桂一鸣), Xu-Sheng Zhang(张徐生), Zi-Jun Liu(刘自军), and Xiang Shen(沈祥)
Chin. Phys. B, 2021, 30 (**9**): 094208. DOI: 10.1088/1674-1056/ac11eb

Design and fabrication of GeAsSeS chalcogenide waveguides with thermal annealing

Limeng Zhang(张李萌), Jinbo Chen(陈锦波), Jierong Gu(顾杰荣), Yixiao Gao(高一骁), Xiang Shen(沈祥), Yimin Chen(陈益敏), and Tiefeng Xu(徐铁峰)
Chin. Phys. B, 2021, 30 (**3**): 034210. DOI: 10.1088/1674-1056/abd757

Experimental and numerical investigation of mid-infrared laser in Pr^{3+}-doped chalcogenide fiber

Hua Chen(陈华), Ke-Lun Xia(夏克伦), Zi-Jun Liu(刘自军), Xun-Si Wang(王训四), Xiang-Hua Zhang(章向华), Yin-Sheng Xu(许银生), Shi-Xun Dai(戴世勋)
Chin. Phys. B, 2019, 28 (**2**): 024209. DOI: 10.1088/1674-1056/28/2/024209

Research progress of third-order optical nonlinearity of chalcogenide glasses

Xiao-Yu Zhang(张潇予), Fei-Fei Chen(陈飞飞), Xiang-Hua Zhang(章向华), Wei Ji(季伟)
Chin. Phys. B, 2018, 27 (**8**): 084208. DOI: 10.1088/1674-1056/27/8/084208

Third-order nonlinear wavelength conversion in chalcogenide glass waveguides towards mid-infrared photonics

Fengbo Han(韩锋博)[1,2], Jiaxin Gu(顾佳新)[2], Lu Huang(黄璐)[1], Hang Wang(王航)[1], Yali Huang(黄雅莉)[2], Xuecheng Zhou(周学成)[1], Shaoliang Yu(虞绍良)[2], Zhengqian Luo(罗正钱)[1], Zhipeng Dong(董志鹏)[1,†], and Qingyang Du(杜清扬)[2,‡]

[1] *Fujian Key Laboratory of Ultrafast Laser Technology and Applications, Xiamen University, Xiamen* 361005, *China*
[2] *Zhejiang Laboratory, Hangzhou* 311100, *China*

(Received 27 May 2024; revised manuscript received 5 July 2024; accepted manuscript online 19 July 2024)

The increasing demand in spectroscopy and sensing calls for infrared (mid-IR) light sources. Here, we theoretically investigate nonlinear wavelength conversion of $Ge_{28}Sb_{12}Se_{60}$ chalcogenide glass waveguide in the mid-IR spectral regime. With waveguide dispersion engineering, we predict generation of over an octave wavelength (2.8 μm–5.9 μm) tuning range Raman soliton self-frequency shift, over 2.5 octaves wavelength cover range supercontinuum (1.2 μm–8.0 μm), as well as single soliton Kerr comb generated in suspended $Ge_{28}Sb_{12}Se_{60}$ waveguide. Our findings evidenced that $Ge_{28}Sb_{12}Se_{60}$ chalcogenide glass waveguides can simultaneously satisfy the generation of Raman soliton self-frequency shift, supercontinuum spectrum, and Kerr frequency comb generation through dispersion engineering towards mid-IR on chip.

Keywords: chalcogenide glass, Raman soliton self-frequency shift, supercontinuum, soliton Kerr comb

PACS: 42.65.Dr, 74.70.Xa, 05.45.–a **DOI:** 10.1088/1674-1056/ad6557

1. Introduction

With the fast development of photonic integrated circuit technology, the photonic industry is seeking on-chip solutions towards large integration density, and low-cost manufacturing. In addition to the telecommunication wavelength range where silicon photonics thrive, this is also same trend in the mid-infrared (mid-IR) regime, where applications such as free space communication, spectroscopic sensing, and hyperspectral imaging locate.[1–8] Specifically, in molecular sensing, a broadband or wavelength tunable light source is generally indispensable. Such a tunable source can be acquired by integrating quantum cascade lasers (QCLs) on-chip; however, its tuning range are greatly limited.[9,10] Integrating Van der Waals material such as black phosphors exhibits potentials in tunable mid-IR lasing.[11,12] Yet, wavelength tuning depends on the cavity geometry and material thickness which are not post-fabrication adjustable. There is, however, another important technology that leverages nonlinear wavelength conversion mechanisms. It converts a pump light, either a femto-second (fs) pulse or a continuous wave (CW) laser and expands its wavelength spread through Kerr and/or other nonparametric processes.[13–18] In fact, such technology has already been widely adopted in near-IR fiber-based light sources.[19–21] However, its implementation in the mid-IR still lacks investigation. The major challenge lies in the absorption of commonly used waveguiding material silicon dioxide and silicon nitride materials beyond 5 μm.[22] Germanium requires molecular beam epitaxy growth, which is a complex and expensive process.[23]

Chalcogenide glass stands out as a suitable material for waveguide choice owing to its large transparent window starting from 1 μm extending beyond 10 μm.[24] Moreover, it has a large nonlinear coefficient comparable to that in silicon with negligible two-photon absorption.[25,26] The amorphous nature of chalcogenide glass further facilitates its large integration onto silicon wafers via mature physical vapor deposition technologies. Indeed, chalcogenide glass waveguide and its optical nonlinearity has been explored and experimentally demonstrated in various spectral ranges.[27–32] However, chalcogenide glass containing arsenic is highly toxic and prone to oxidation under environmental conditions, resulting in unstable performance, and most importantly, drifting refractive index resulted from photodarkening effect. Consequently, changing in refractive index alters its dispersion behavior, thus deteriorating supercontinuum performance over time, such as As–S[27,28,31] and Ge–As–Se–S.[33] Replacing As with heavier Sb atoms for $Ge_{28}Sb_{12}Se_{60}$ (GeSbSe) chalcogenide glass can solve these problems, not only inheriting strong optical properties, but also making the material non-toxic and more stable. Compared to Ge–Sb–S, GeSbSe has higher refractive index and nonlinear coefficient, which means higher integration and more favorable nonlinear effects.

In this article, we aim to present a systematic theoretical investigation on its potential to achieve broadband or wavelength tunable laser source toward mid-IR leveraging third or-

†Corresponding author. E-mail: zpdong@xmu.edu.cn
‡Corresponding author. E-mail: qydu@zhejianglab.edu.cn

© 2024 Chinese Physical Society and IOP Publishing Ltd

der nonlinearities. By carefully engineering GeSbSe waveguide dispersion, chalcogenide glass waveguides are able to produce supercontinuum expanding over 2.5 octaves, Raman soliton with center wavelength continuously tunable over an octave as well as stable Kerr soliton combs. Our findings provide a useful design guideline for nonlinear mid-IR chalcogenide glass photonics, which can simultaneously satisfy Raman soliton self-frequency shift, supercontinuum, and Kerr frequency comb generation.

2. Dispersion engineering in waveguide

To maximize the nonlinear wavelength conversion effect, phase matching is the key requirement. In general, highly efficient nonlinear wavelength conversion occurs in the vicinity of the zero dispersion wavelengths (ZDWs), for the reason that the converted light will be able to interfere constructively and accumulate in intensity. The light pulse wavelength span/tunable range is further determined by the flatness of the dispersion curve. Therefore, our goal is to engineer the waveguide dispersion towards a flat curve with small dispersion. Specifically, we take chalcogenide glass with composition GeSbSe, also commercially available as IG5, as our waveguide. And the FOM $= n_2/(\beta\lambda)$[34] of GeSbSe's nonlinear material is 548, which indicates higher nonlinear conversion efficiency. It is transparent in the mid-IR all the way to 11 μm, and its large nonlinear optical coefficient guaranteed low pump threshold energy. In addition, the arsenic-free composition further immunes the material from oxidation at room temperature, facilitating its fabrication and handling. In order to completely eliminate any material absorption such as cladding, we cut the silicon dioxide bottom undercladding to form a suspended rib waveguide, which not only provides greater optical confinement but also better waveguide dispersion control.[35] A schematic drawing of the waveguide structure is presented in Fig. 1(a), where we denote H as the waveguide rib height, T as the slab thickness, and W as the waveguide width. The two arrays of holes in the vicinity of the rib allows wet etchant penetrating to undercut the buried oxide. The three waveguide parameters are surveyed to find their influence on the waveguide group velocity dispersion (GVD). Figures 1(b)–1(d) show the calculated GVD curves of the fundamental TE mode by varying W, H, and T, respectively. The material refractive index curve is directly quoted from previously experimentally measured result from an IR ellipsometer.[30] The GVD clearly indicates that our suspended waveguide structure has two ZDWs, which is beneficial for engineering a flat curve. In contrast to the waveguide width which does not impact the GVD curves (Fig. 1(b)), increasing total waveguide height pushes the second ZDW towards longer wavelengths, simultaneously enhancing the total anomalous GVD value (Fig. 1(c)). However, such effect could be mitigated by making the slab thick (Fig. 1(d)). For applications that require to maintain a low dispersion, a relatively thick slab is preferred. Otherwise, a high rib to slab ratio waveguide is recommended. However, mechanical stability must be taking into concern for this type of waveguide. Studies have shown that a ratio below 4:1 is in general sufficiently robust enough to support such suspended structure.[36]

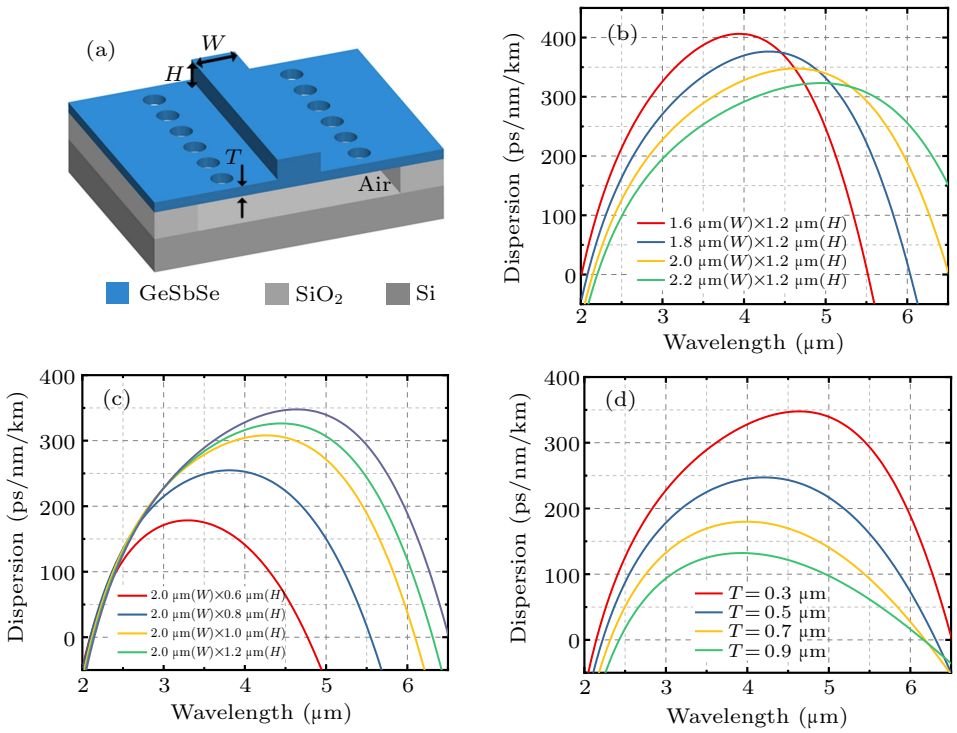


Fig. 1. (a) A schematic drawing suspended waveguide structure; (b)–(d) waveguide dispersion curve of varying width (fixed $T = 0.3$ μm), height (fixed $T = 0.3$ μm), and slab thickness (fixed $W = 2$ μm, $H = 1.1$ μm), respectively.

3. Nonlinear wavelength conversion

The nonlinear dynamics of an optical pulse in waveguide is governed by the generalized nonlinear Schrödinger equation (GNLSE), which takes the following form:[37]

$$\frac{\partial A}{\partial z}+\frac{1}{2}\left(\alpha(\omega_0)+\mathrm{i}\alpha_1\frac{\partial}{\partial t}\right)A-\mathrm{i}\sum_{n=1}^{\infty}\frac{\mathrm{i}^n\beta_n}{n!}\frac{\partial^n A}{\partial t^n}$$
$$=\mathrm{i}\left(\gamma(\omega_0)+\mathrm{i}\gamma_1\frac{\partial}{\partial t}\right)A(z,t)$$
$$\times\int_0^{\infty}R(t')\left|A(z,t-t')\right|^2\mathrm{d}t', \tag{1}$$

where A represents the envelop evolution of the optical pulse, α stands for the propagation loss, β_n is the n-th orders of dispersion coefficient. The right-hand side of the equation considers possible nonlinear effect. γ stands for the nonlinear coefficient, and $R(t)$ is the nonlinear response function, which includes both contributions from electrons and nucleus. It is expressed as

$$R(t)=(1-f_{\mathrm{R}})\,\delta(t)+f_{\mathrm{R}}h_{\mathrm{R}}(t), \tag{2}$$

where f_{R} denotes the fractional contribution of the delayed Raman response to nonlinear polarization, and $h_{\mathrm{R}}(t)$ is the Raman response function. Both are material dependent parameters. Numerically solving the GNLSE provides the pulse evolution and nonlinear wavelength conversion dynamics.

3.1. Raman soliton self-frequency shift (SSFS)

It has been well established that a reasonable amount of anomalous dispersion for the pump soliton pulse is necessary to initiate Raman SSFS. We therefore choose GeSbSe waveguide ($\alpha=3$ dB/cm) with dimensions $W=2.0$ μm, $H=1.1$ μm, $T=0.3$ μm, as shown in Fig. 2(a), whose dispersion curve is represented by the red line in Fig. 1(d). A 100-fs laser pump pulse with center wavelength at 2.8 μm is chosen to fully explore SSFS effects in the mid-IR. We conduct the simulation by numerically solve GNLSE using previously established split step Fourier transform protocol.[33] The results of the generated SSFS with respect to the pump pulse energy and its corresponding temporal evolution are plotted in Figs. 2(b) and 2(c), respectively. At a threshold energy of 7 pJ, SSFS starts to be observed. As the pump energy increases to 200 pJ, the center wavelength of the SSFS shifting from 2.8 μm and reaches 5.9 μm, creating larger than one octave tuning range. It is interesting to note that the soliton shape becomes broader after the pump pulse is beyond 150 pJ, whose center wavelength also coincides with the maximum point of the waveguide's GVD curves. This is primarily due to the fact that with dispersion diminishes, nonlinear effect of spectral broadening begins to dominate, and therefore the created soliton are more spectrally spread.

Next, we investigate its soliton dynamics as is given in Figs. 3(a) and 3(b). After propagating a waveguide length of 5 mm, a distinctive soliton branch separates from the pump and begins red shifting until passing a length of 10 mm. After that, the soliton balances its dispersion with nonlinearity and reshapes. It is also evident that more than one soliton as well as dispersive waves are generated in this process, which is also observable in Fig. 2(b). We then further calculated the conversion efficiency of SSFS and plotted in Fig. 3(c). The results clearly show the efficiency is greater than 50%, regardless of the pump pulse energy.

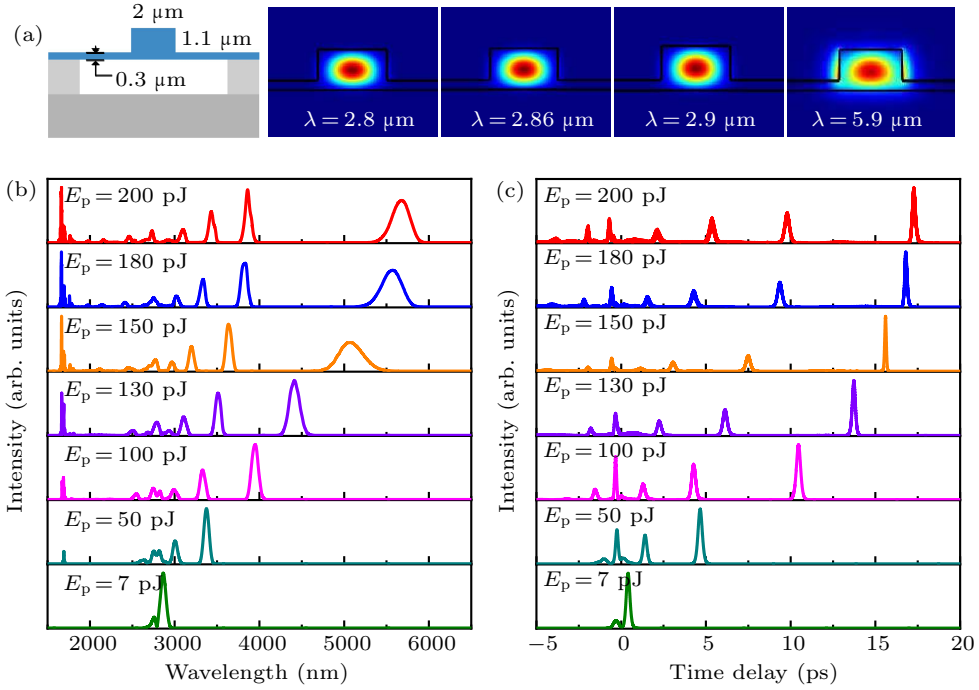


Fig. 2. (a) Illustration of waveguide structure for Raman SSFS, (b) spectral, and (c) temporal evolutions of SSFS with increasing pump power.

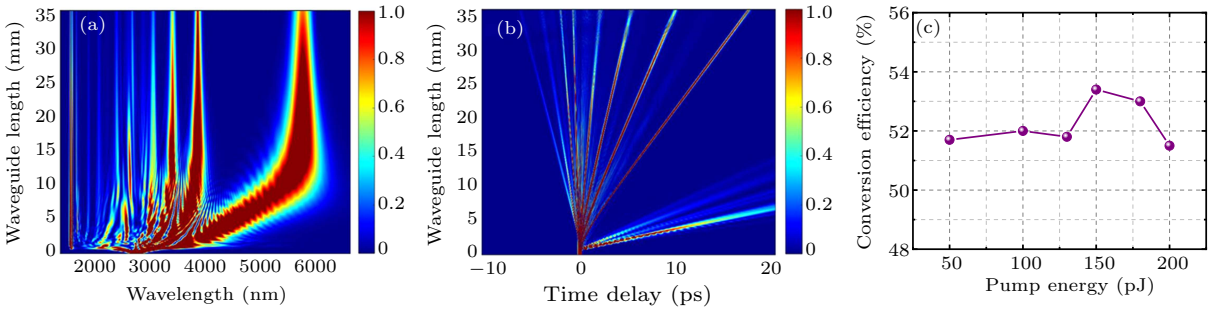


Fig. 3. (a) Spectral and (b) temporal evolutions of the pump soliton pulse along waveguide propagation, (c) pump soliton conversion efficiency to SSFS under various pump energies.

3.2. Supercontinuum generation

Supercontinuum is another nonlinear wavelength conversion process. Unlike SSFS that carefully shifts the soliton central wavelength towards longer wavelengths, supercontinuum expands the pump laser and creates a spectrally ultrabroadband pulse. It involves multiple nonlinear mechanisms such as soliton fission, self-phase modulation, four-wave mixing, intra-pulse Raman scattering as well as dispersive wave generation. To effectively generate supercontinuum, a flat curve with low dispersion value is required to meet the phase matching condition. The waveguide ($\alpha = 1$ dB/cm) structure is then designed to be $W = 3.0$ μm, $H = 1.0$ μm, $T = 0.7$ μm, whose dispersion curve and structure are illustrated in Fig. 4(a). To generate a supercontinuum with maximum possible spread, we pumped the waveguide at the anomalous dispersion side of the ZDW. The same pump pulse parameter as the one in SSFS (100 fs, 2.8 μm, and 200 pJ) are injected. Figures 4(b) and 4(c) display its spectral expansion and evolution after passing 10-mm long waveguide, respectively. Significant spectral broadening of over an octave is achieved after 50-pJ pump power. As the pump power continues to increase, the supercontinuum expands starting from 1.2 μm and passing beyond 8 μm, covering over 2.5 octaves. Its evolution map also indicates that fission of the soliton pulse occurs at a waveguide length of 10 mm. Subsequently, the solitons shift their center wavelengths, broaden their spectral width, and finally connect to form a consecutive ultrabroadband pulse. Our waveguide structure has evidenced its superior ability in achieving super broadband mid-IR light source.

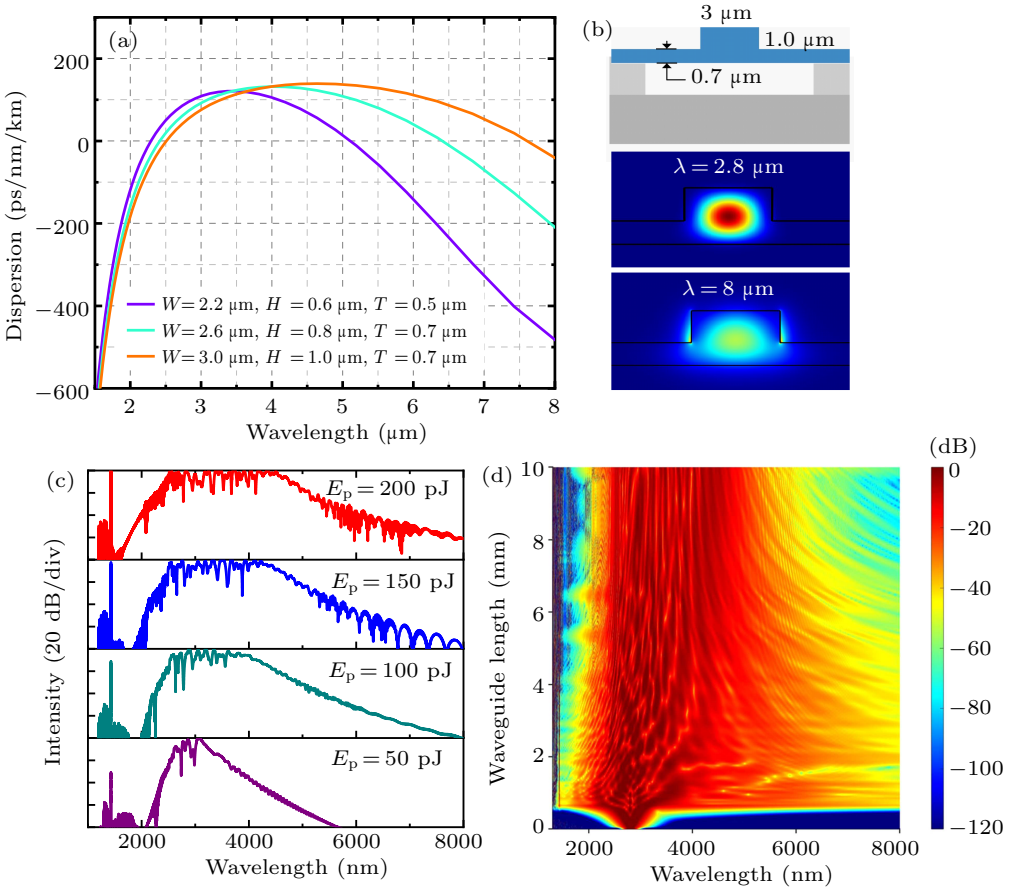


Fig. 4. (a) Illustration of waveguide structure for supercontinuum generation and their corresponding dispersion curve, (b) supercontinuum generation under increasing pump energy, and (c) spectral evolution of supercontinuum pulse.

3.3. Kerr soliton micro-comb generation

In addition to directly pumping in a waveguide, Kerr soliton comb leverages strong cavity field enhancement effect in high-Q whispering gallery resonant mode. It excites a greater number of oscillating modes through four-wave mixing and forms a stable soliton envelop. The modal field dynamics are characterized by a spatiotemporal formalism known as Lugiato–Lefever equation (LLE), an intra-cavity azimuthal representation of the GNLSE.[38] It takes the form of

$$\frac{\partial \psi(\theta,\tau)}{\mathrm{d}\tau} = -(1+\mathrm{i}\delta)\psi + \mathrm{i}|\psi|^2\psi - \mathrm{i}\frac{B}{2}\frac{\partial^2\psi}{\partial\theta^2} + F. \tag{3}$$

The $\tau = t/\tau_{\mathrm{ph}}$ here represents the time normalized by the photon life time, δ is the frequency detuning normalized by cavity loaded FWHM, and B is the normalized GVD.

$$\delta = -\frac{2(\Omega_0-\omega_0)}{\Delta\omega_{\mathrm{tot}}}, \quad B = -\frac{2\beta_2}{\Delta\omega_{\mathrm{tot}}}, \tag{4}$$

where $\Delta\omega_{\mathrm{tot}}$ denotes the FWHM of the loaded cavity resonance. F is the external pump term

$$F = \sqrt{\frac{8g_0\Delta\omega_{\mathrm{ext}}}{\Delta\omega_{\mathrm{tot}}^3}\frac{P}{\hbar\Omega_0}}. \tag{5}$$

Here, $g_0 = n_2 c\hbar\Omega_0^2/(n_0^2 V_0)$ is the nonlinear gain where n_0 and n_2 are the linear and nonlinear refractive indices, V_0 is the modal volume, P denotes the external pump, and $\Delta\omega_{\mathrm{ext}}$ is the coupling-Q-related FWHM.

To numerically solve LLE, the dispersion term is expressed with respect to cavity resonance mode. The frequency of the relative mode number μ can be expressed as the Taylor expansion around the center frequency Ω_0, yielding a linear dispersion D_1 and integrated higher order dispersion D_{int}

$$\begin{aligned}\omega_\mu &= \omega_0 + D_1\mu + \frac{1}{2}D_2\mu^2 + \frac{1}{6}D_3\mu^3 + \frac{1}{24}D_4\mu^4 + \cdots \\ &= \mathrm{i}\omega_0 + D_1\mu + D_{\mathrm{int}}.\end{aligned} \tag{6}$$

We designed a micro-resonator with a ring radius of 250 μm under the same geometry, its second-order dispersion and integrated dispersion D_{int} of both TE and TM modes are plotted in Figs. 5(a) and 5(b), respectively. The pump wavelength of 2.8 μm is selected to coincide with the zero dispersion of D_{int}. By setting a loaded-Q factor of the resonator to be 9×10^5, the corresponding waveguide propagation loss α of 0.8 dB/cm, and a pump power of 28.5 mW, our simulation results yield a single Kerr soliton formed inside the micro-resonator with wavelength spanning from 2.62 μm to 2.98 μm, which are illustrated in Figs. 5(c) and 5(d). The comb teeth spacing is 1.76 nm, and their ensemble establishes a sech_2 envelop, evidencing the comb's soliton behavior. It is worth emphasizing that multiple soliton comb and modulation instability comb states are also solutions to the LLE, by carefully adjusting the pump wavelength detuning, such states are accessible. The wavelength spanning can be expanded by further dispersion engineering (i.e., waveguide width, height, and slab thickness) and increasing the pump power. The generated mid-IR soliton combs have great potential in ultrafast ranging and detection as well as dual comb spectroscopy for molecular sensing.[6,39]

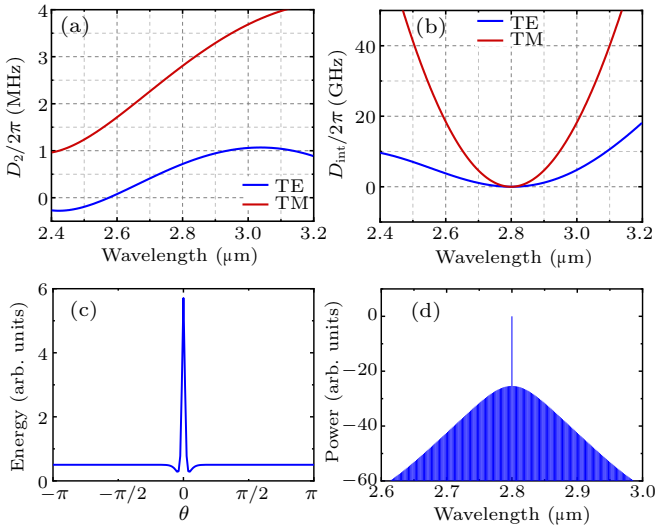


Fig. 5. (a) The second order and (b) the integrated dispersion curves for TE and TM polarization in a micro-ring cavity resonator, (c) the azimuthal field distribution of the cavity, and (d) a soliton micro-comb spectrum generated from the resonator.

4. Discussion

While it is obvious from mathematical equations that CW laser-pumped parametric processes require stringent phase matching condition, managing dispersion is also vital in ultrafast pulse evolutions. For SSFS, a certain abnormal dispersion is needed to maintain the soliton state. We further simulated SSFS process at an even higher abnormal dispersion at a pump wavelength of 2.9 μm, as shown in Fig. 6(a). The soliton conversion efficiency of 2.9-μm pump wavelength is lower than that of 2.8 μm, the soliton conversion efficiency is 47.2% when the pump energy is 200 pJ. By comparing with Fig. 2(b), it can be seen that at longer SSFS center wavelength, a higher pump power is demanded to balance the large initial dispersion. It is also interesting to point out that pumping close to ZDW does not promote SSFS for the reason that small dispersion no longer supports soliton state which consequently fissions into supercontinuum. Similarly, pumping at the normal dispersion side of the ZDW also yields different forms of supercontinuum. Plotted in Fig. 6(b) is the simulation result of pumping wavelength of 2.45 μm for waveguide structure as shown in Fig. 4(a). Instead of undergoing soliton fission process, the pump pulse broadens its wavelength span via self-phase modulation, forming a flat-top supercontinuum. The wavelength covers from 1.2 μm to 5.5 μm narrower compared with the results in Fig. 4(a) but is highly coherent, which is advantageous

under coherence-required application. Therefore, in addition to choosing a waveguide material with high nonlinearity and low absorption, dispersion engineering is another key factor in achieving efficient nonlinear wavelength conversion.

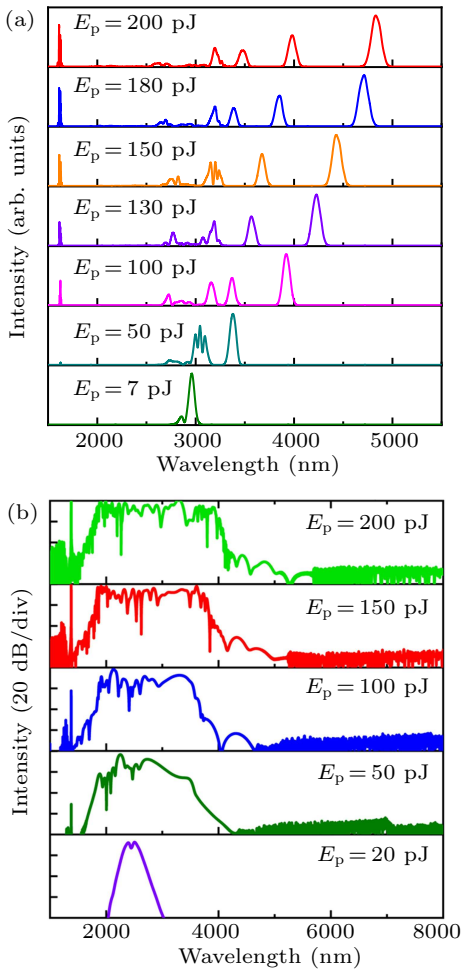


Fig. 6. (a) SSFS evolution pumped at higher abnormal dispersion and (b) a flat-top supercontinuum generation pumped at normal dispersion.

5. Conclusion

To sum up, we proposed a suspended mid-IR nonlinear waveguide by transparent and highly nonlinear material GeSbSe. Through waveguide geometry dispersion engineering, we successfully predicted such waveguide capable of producing continuous wavelength tuning Raman soliton from 2.8 μm to 5.9 μm, 2.5 octaves wavelength spanning supercontinuum from 1.2 μm to 8.0 μm, and micro-resonator single soliton Kerr comb. GeSbSe waveguides with loss down to 0.8 dB/cm have been fabricated in our recent work,[40] which will make generation of such braodband supercontinuum, SSFS, and Kerr soliton possible in the future. Our result clearly evidenced GeSbSe suspended waveguide with strong nonlinear optics capability in the mid-IR spectral regimes.

Acknowledgments

Project supported by the National Natural Science Foundation of China (Grant Nos. 62105272 and 62305304), the Natural Science Foundation of Fujian Province, China (Grant Nos. 2022J06016 and 2021J05016), the National Key Research and Development Program of China (Grant No. 2021ZD0109904), the Key Research Project of Zhejiang Laboratory (Grant No. 2022PH0AC03), and the Fundamental Research Funds for the Central Universities (Grant No. 20720220109).

References

[1] Hu J J, Meyer J and Richardson K 2013 *Opt. Mater. Express* **3** 1571
[2] Milosevic M, Nedeljkovic M and Masaud T 2012 *Appl. Phys. Lett.* **101** 121105
[3] Zou K, Pang K and Song J 2022 *Nat. Commun.* **13** 7662
[4] Rosi F, Miliani R and Braun R 2013 *Angew. Chem.* **52** 5258
[5] Junaid S, Kumar S and Mathez M 2019 *Optica* **6** 702
[6] Luo P and Chen I 2022 *Optica* **94** 5752
[7] Ma P, Choi D and Yu Y 2013 *Opt. Express* **21** 29927
[8] Han Z, Lin P and Singh 2016 *Opt. Express* **108** 141106
[9] Tsay C, Toor F and Gmachl C 2010 *Opt. Lett.* **35** 3324
[10] Nicoletti S, Fedeli J and Fournier M 2019 *Silicon Photonics XIV* **10923** 109230H
[11] Chang T, Chen Y and Luo D 2019 *Nano Lett.* **20** 6824
[12] Zhang Y, Wang S and Chen S 2020 *Adv. Mater.* **32** 1808319
[13] Kuyken B, Ideguchi T and Holzner S 2014 *Nat. Commun.* **6** 6310
[14] Luke K, Okawachi Y and Lamont M 2015 *Opt. Lett.* **21** 40
[15] Griffith A, Lau R and Cardenas J 2014 *Nat. Commun.* **6** 6299
[16] Ettabib M, Xu L, Bogris A and Petropoulos P 2015 *Opt. Lett.* **40** 4118
[17] Rong H, Jones R, Liu A and Cohen O 2005 *Nature* **433** 725
[18] Zlatanovic S, Park J, Moro S and Radic S 2010 *Nat. Photon.* **4** 561
[19] Zhou J, Pan W, Qi W, Cao X, Cheng Z and Feng Y 2022 *PhotonicX* **3** 18
[20] Li H, Li X, Zhang S, Yan D, Wang C, Yang Z and Pang Z 2023 *Opt. Laser Technol.* **163** 109336
[21] Huang J, Lu Y, Wu Z, Xie Y, He C and Wu J 2022 *Chin. Opt. Lett.* **20** 031902
[22] Lin H, Luo Z, Gu T, Kimerling L, Wada K, Agarwal A and Hu J 2022 *Nanophotonics* **7** 393
[23] Mtunzi M, Jia H, Hou Y and Yu X 2022 *J. Phys. D: Appl. Phys.* **57** 255101
[24] Eggleton B, Luther-Davies B and Richardson K 2011 *Nat. Photon.* **5** 141
[25] Zhang L, Chen J, Gu J, Gao Y, Shen X, Chen Y and Xu T 2021 *Chin. Phys. B* **30** 034210
[26] Wang H, Wu B and Wang X 2015 *Chin. Phys. B* **25** 064207
[27] Yu Y, Gai X, Ma P, Choi D, Yang Z, Wang R, Debbarma S, Madden S and Luther-Davies B 2014 *Laser Photon. Rev.* **8** 792
[28] Gai X, Choi D, Madden S, Yang Z, Wang R and Luther-Davies B 2012 *Opt. Lett.* **37** 3870
[29] Xia D, Yang Z, Zeng P and Li Z 2022 *Laser Photon. Rev.* **17** 2200219
[30] Li Z, Du Q, Wang C, Zou J, Du T, Richardson K, Cai Z, Hu J and Luo Z 2020 *Laser Photon. Rev.* **15** 2000301
[31] Lamont M, Luther-Davies B, Choi D, Madden S and Eggleton B 2008 *Opt. Express* **16** 14938
[32] Karim M, Ahmad H, Ghosh S and Rahman B 2018 *J. Appl. Phys.* **123** 213101
[33] Alekberov R, Mekhtiyeva S and Mammadov S 2024 *J. Korean Phys. Soc.* **84** 694
[34] Zhang X, Chen F, Zhang X and Ji W 2018 *Chin. Phys. B* **27** 084208
[35] Li Z, Han F, Dong Z, Du Q and Luo Z 2021 *Opt. Express* **30** 25356
[36] Xia Y, Qiu C, Zhang X, Gao W, Shu J and Xu Q 2013 *Opt. Lett.* **38** 11224
[37] Godey C, Balakireva I, Coillet A and Chembo Y 2013 *Phys. Rev. A* **89** 063814
[38] Younas U, Sulaiman T and Ren J 2023 *Opt. Quantum Electron.* **55** 72
[39] Trocha P, Ganin D, Karpov M, Pfeiffer M, Kordts A and Krockenberger J 2018 *Opt. Lett.* **359** 887
[40] Han F, Niu Y, Zhang Y, Gong J, Yu S and Du Q 2024 *J. Phys. D: Appl. Phys.* **57** 305107